catalysts

MDPI

Article

Limestone Calcination Kinetics in Microfluidized Bed Thermogravimetric Analysis (MFB-TGA) for Calcium Looping

Dan Li, Yang Wang and Zhenshan Li *

Key Laboratory for Thermal Science and Power Engineering of Ministry of Education, Department of Energy and Power Engineering, Tsinghua University, Beijing 100084, China
* Correspondence: lizs@mail.tsinghua.edu.cn; Tel.: +86-10-62789955

Abstract: Limestone calcination is an important part of calcium looping (CaL) technology and is critical to the design and operation optimization of fluidized bed reactors. However, obtaining a method of measuring the fast calcination kinetics in a fluidizing environment with isothermal conditions is still a challenge in the field of calcium looping. We address this challenge in this work and develop a new method of obtaining limestone calcination kinetics by injecting limestone particles into the hot fluidizing sands in a microfluidized bed thermogravimetric analysis (MFB-TGA) with a mass measurement resolution of 1 mg. The calcination characteristics of limestone are investigated at different particle sizes (150–1250 μm), temperatures (750–920 °C), and CO_2 concentrations (0–30 vol.%). The experimental data measured from MFB-TGA were analyzed using a detailed model including surface reaction and intraparticle and external diffusion. The results show that the kinetics of limestone calcination measured by MFB-TGA are faster than those measured via regular TGA. This particle-injecting method of MFB-TGA provides a new experimental idea for measuring fast calcination kinetics occurring inside fluidized bed reactors and provides guidance on the application of CaL technology.

Keywords: limestone calcination; microfluidized bed thermogravimetric analysis (MFB-TGA); calcination kinetics; model

check for updates

Citation: Li, D.; Wang, Y.; Li, Z. Limestone Calcination Kinetics in Microfluidized Bed Thermogravimetric Analysis (MFB-TGA) for Calcium Looping. *Catalysts* **2022**, *12*, 1661. https://doi.org/10.3390/catal12121661

Academic Editors: Chuande Huang, Bo Jiang, Xin Tian and Jiawei Hu

Received: 16 November 2022
Accepted: 14 December 2022
Published: 17 December 2022

Publisher's Note: MDPI stays neutral with regard to jurisdictional claims in published maps and institutional affiliations.

Copyright: © 2022 by the authors. Licensee MDPI, Basel, Switzerland. This article is an open access article distributed under the terms and conditions of the Creative Commons Attribution (CC BY) license (https://creativecommons.org/licenses/by/4.0/).

1. Introduction

Calcium looping technology is a promising technology based on the calcination/carbonation reaction of calcium carbonate ($CaCO_3$) [1,2]. It can be widely applied in carbon capture, adsorption-enhanced steam methane reforming (SE-SMR), integrated CO_2 capture and conversion, and thermochemical heat storage [3–7]. CaL technology typically involves the use of dual interconnected circulating fluidized bed (CFB) reactors [8,9]. In the first reactor, lime (CaO) reacts with CO_2 in the temperature range of 600–700 °C to form $CaCO_3$. The $CaCO_3$ is then subsequently transported to the second CFB reactor for calcination. The regenerated CaO is then looped back to the first reactor. CaL technology has the following advantages [10,11]: abundant and inexpensive natural limestone with high theoretical CO_2 capture capacity and relatively low energy consumption; high energy storage density and great heat recovery potential due to high-temperature carbonation reaction. The $CaCO_3$ calcination stage, as a major part of the CaL technology, has a significant influence on the design and operation of the regeneration reactor, system integration and optimization, and the sintering of the CaO absorbent [12,13].

$CaCO_3$ calcination is a complex physical and chemical process in which reaction, heat transfer, and mass transfer are mutually coupled [14]. Researchers have studied the influence mechanism of $CaCO_3$ calcination, and it is generally accepted that with a decrease in particle size, the influence of heat transfer on calcination kinetics weakens and the influence of chemical reaction enhances [15–17]. For very small particles (<90 μm), the chemical reaction is the controlling step [17]. For particles >6 mm, heat transfer

becomes a key process [18]. For the particle size between these values, both chemical reaction and mass transfer control the calcination kinetics [19]. Several models have been developed in the past to describe the calcination behavior, including the shrinking core model [20], the grain model [21], the uniform transformation model [17], and the random pore model [15]. The calcination of $CaCO_3$ particles with low porosity has been typically described using the shrinking core model, which assumes that there is an obvious reaction interface between the nonporous $CaCO_3$ and the generated CaO [19,20,22]. However, the diffusion of generated CO_2 through the CaO layer and external diffusion processes in the atmosphere are generally ignored. Diffusion resistance has an important influence on the decomposition of kinetics, especially for larger particle sizes [23]. In addition, due to several factors affecting the calcination of $CaCO_3$, such as particle size, temperature, CO_2 concentration, and experimental apparatus, there is no consensus on the calcination mechanism of $CaCO_3$ particles, and the obtained kinetic parameters are markedly different. It has been reported [24–26] that the activation energy of $CaCO_3$ calcination is in the range of 100–230 kJ/mol. Furthermore, researchers [19,27–29] have found that the CO_2 concentration in the atmosphere has a significant effect on the $CaCO_3$ calcination rate. The effect of CO_2 partial pressure on the calcination is normally described with the form of $(1 - P/P_{eq})^n$ (where P is the CO_2 partial pressure in the atmosphere and P_{eq} is the CO_2 equilibrium partial pressure), and the value of the exponent n ranges from 0.5 to 2 [19,30,31]. Some researchers adopt surface elementary reactions to explain the chemical reaction kinetics of $CaCO_3$ calcination in CO_2 atmosphere [19,32,33]. The broad activation energy and CO_2 partial pressure ranges reveal that calcination experiments and modeling under fluidized bed conditions are of great significance for the future scaling up of CaL technology. Regardless of the concept used for describing the calcination kinetics, the calcination data must be measured based on an accurate experimental method.

In order to obtain the kinetics of $CaCO_3$ calcination, there are mainly the following methods: (i) Thermogravimetric analyzer (TGA) is a method commonly adopted by researchers [22,25,29,34–36]. However, it is still a challenge to obtain calcination results at constant temperatures [36], especially at high temperatures. In addition, the heating rate of particles is usually lower than 100 K/min, and the diffusion resistance is serious in TGA instruments, which is not conducive to the development of kinetics models. The solid sample in the crucible of TGA is in a packed state, which is somewhat different from the fluidization in a fluidized reactor. (ii) Fluidized bed reactor based on gas signal measurement [27]. The vigorous movement of solid particles means excellent heat and mass transfer, which is a natural advantage of fluidized bed reactors for kinetic studies. The difficulty of the method lies in the capture of minor change in the gas concentration signal of rapid reaction, especially when the CO_2 produced by the sample is very little at high CO_2 concentrations [37]. Moreover, the blend of gas species affects the original signal and causes errors when there are variations in the concentration of multiple constituent gases in the experiment. (iii) Tube furnace [38] and high-temperature gas–solid suspension furnace [39,40]; the particle heating rate is fast, but the sample size is smaller than ~70 μm, and the residence time is shorter than 5 s. At the same time, the gas and particles inside the drop tube furnace are in entrained flow, while the gas inside the fluidized bed is divided into a bubble phase and an emulsion phase. The particles inside the fluidized bed will form a dense phase. Therefore, the calcination kinetics obtained from drop tube furnace cannot be accurately applied for the development of a fluidized bed reactor. (iv) In situ XRD method [32]; the change in crystal structure of $CaCO_3$ particles during calcination is analyzed using X-ray diffraction, which can be combined with TGA to obtain in situ particle conversion.

Limestone calcination for calcium looping occurs in a fluidizing state; therefore, it is necessary to measure the calcination kinetic data from the fluidized bed reactor. The aim of the work is to obtain the limestone calcination characteristics in the fluidized bed condition and to describe the calcination kinetics to guide the design and operation scale-up of the fluidized bed reactor. First, based on the previously constructed MFB-TGA with a mass

measurement resolution of 1 mg and strong heat and mass transfer properties [41], a new method of injecting the limestone particles into the MFB-TGA is proposed and developed to measure the calcination kinetics under the fluidization and isothermal conditions with various particle sizes, temperatures, and CO_2 partial pressures under constant temperature conditions. Then, a shrinking core model is established considering the effects of CO_2 concentration and mass transfer rate on the calcination process. Finally, the relative importance of surface reactions, intraparticle diffusion, and external gas diffusion is analyzed and discussed based on experimental data and established models.

2. Results

2.1. Comparison of MFB-TGA with Regular TGA

TGA is a commonly used commercial instrument for measuring the kinetics of limestone calcination [22,25,29,35]. In the TGA experiment, a 5–10 mg sample is placed in a crucible and heated at a heating rate of 50 K/min to obtain the weightless curvature of the limestone. It can be seen from Figure 1 that the limestone particles are decomposed during the heating process. The decomposition characteristics of limestone particles under constant temperature conditions are difficult to obtain, which is of great significance for the establishment of the decomposition models and the determination of kinetics. Furthermore, the conversion of limestone particles in TGA is slower compared to MFB-TGA due to the gas diffusion resistance. Thus, a smaller value of calculated chemical reaction rate constant could be obtained from TGA results. Correspondingly, the controlling step may be wrongly determined as a chemical reaction. It still remains a challenge for the TGA method to eradicate the mass transfer effects and maintain isothermal decomposition, especially for rapid reactions [41,42]. MFB-TGA couples the accurate and real-time quality monitoring characteristics of TGA and the motion state of particle fluidization with good heat and mass transfer effects [27]. The CO_2 produced by the calcination of the 60–70 mg limestone sample is limited. Coupled with the fast external diffusion rate, the effect of mass transfer is significantly reduced. Details on the reduction of mass transfer effects by MFB-TGA can be found in previous works [41,43].

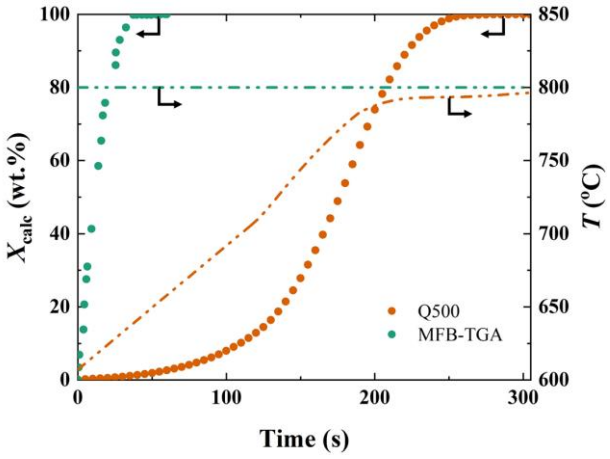

Figure 1. Comparison of MFB-TGA experimental results to TGA (800 °C, 0 vol.% CO_2).

2.2. Effect of Temperature on the Calcination Kinetics

Temperature has a significant effect on the calcination performance of limestone in a broad range. Calcination experiments of limestone with particle sizes of 150 μm are conducted at temperatures from 750 to 920 °C under N_2 atmosphere in MFB-TGA apparatus. The model results are compared with the experimental data of MFB-TGA at various temperatures shown in Figure 2a. The conversion of limestone particles increases rapidly from initial to full conversion with time, especially at high temperature. Under 900 °C, it only takes ~10 s for particle conversion to achieve ~100%. Even at 750 °C, the particle conversion reaches more than 90% in ~60 s, which is significantly faster than the

calcination rate reported in other works [23,25,44]. It is mainly due to the fact that the limestone particles are injected into the quartz reactor in the MFB-TGA experiments. The particles achieve the target temperature and CO_2 concentration in an instant for calcination. In the state of vigorous fluidization, the particles are well blended with the inert bed material, and the temperature of the particles are basically kept consistent with the inert bed material.

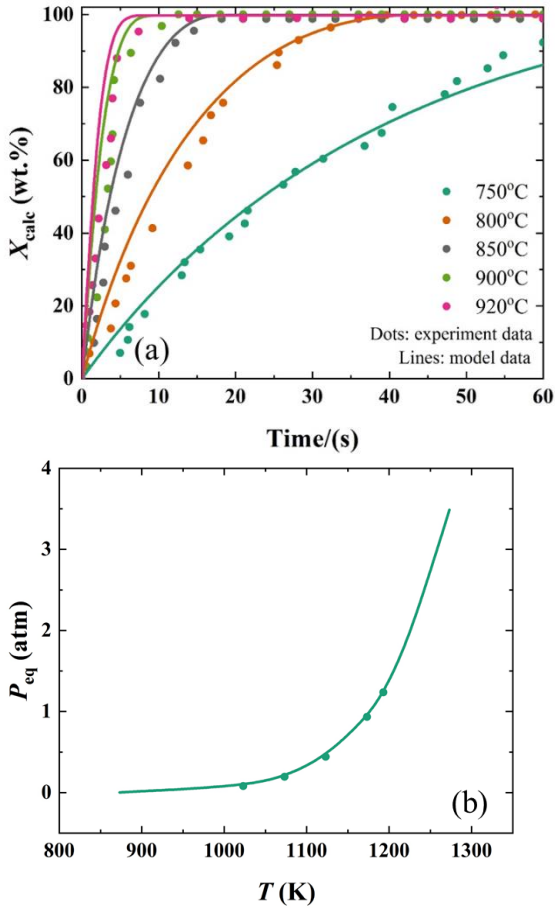

Figure 2. The effect of temperature: (**a**) comparison of model results with MFB-TGA experimental data; (**b**) the relation between CO_2 equilibrium partial pressure and temperature.

The conversion of limestone particles increases significantly with temperature. At 750, 800, 850, 900, and 920 °C, the time for the particle conversion to attain ~90% corresponds to 54 s, 25 s, 15 s, 8 s, and 6 s, respectively. This is mainly attributable to the calcium carbonate calcination reaction being an endothermic reaction with a standard enthalpy of +178 kJ/mol. In addition, as shown in Figure 2b, the thermodynamic equilibrium partial pressure of CO_2 corresponding to calcium carbonate calcination increases exponentially with temperature. Based on Equation (29), the calcination driving force (P_{eq}-P_g) increases, resulting in a gradual increase in the calcination rate. The above discussion indicates that the model can predict well the effect of temperature on calcination characteristics.

2.3. Effect of CO_2 Concentration on the Calcination Kinetics

The effect of CO_2 concentration in the gas phase on the limestone calcination is displayed in Figure 3. With the increase of CO_2 concentration in the gas phase, the conversion of limestone decreases significantly under a certain temperature. At 900 °C, when the CO_2 concentration is 0 vol.%, the particles only require ~11 s to achieve complete conversion, while under 30 vol.% atmosphere, the particle conversion is only 70 wt.% within 80 s. At 920 °C, the particles can be almost completely converted. The calcination rate of lime-

stone under different CO_2 concentrations can be well predicted using the kinetic model established in Section 5.

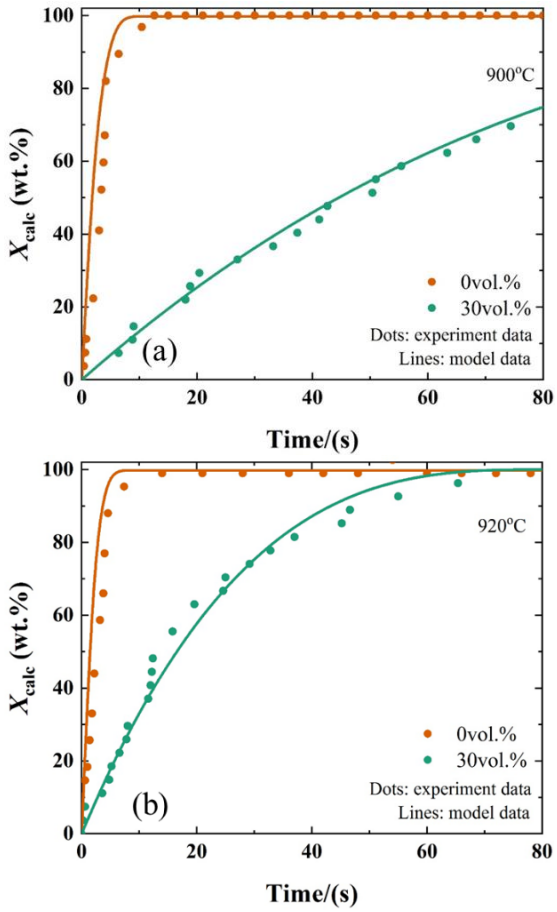

Figure 3. Comparison between the model results and the MFB-TGA experimental data at different CO_2 concentrations under (**a**) 900 °C and (**b**) 920 °C.

The MFB-TGA experiments are conducted under atmospheric pressure, and thus the volume fraction of CO_2 determines the CO_2 partial pressure in the gas phase. It can be obtained from Equation (15) that the partial pressure of CO_2 has a significant effect on the chemical reaction rate of calcium carbonate calcination. With the increase in CO_2 partial pressure P_g in the gas phase from 0 vol.% to 30 vol.% under 900 °C, the comprehensive chemical reaction constant k_c decreases dramatically by ~2 orders, which significantly reduces the calcination rate of limestone particles. With the increase in CO_2 concentration, the intraparticle diffusion rate of CO_2 generated by particle calcination from the reaction surface to the particle surface decreases, especially at the initial stage of the reaction. As the reaction proceeds, the driving force decreases (P_i-P_g), P_i is close to P_g, and the influence of diffusion is no longer significant.

2.4. Effect of Particle Size on the Calcination Kinetics

Particle size is an important factor determining calcination kinetics and generally affects external and intraparticle gas diffusion resistance. Limestone particles of different particle sizes are applied in practice. Thus, it is necessary to investigate the calcination characteristics of particles in different particle size ranges. The calcination process of 150–1250 μm limestone particles under 900 °C and 0 vol.% and 30 vol.% CO_2 concentration is explored in this work. As shown in Figure 4, the limestone particles conversion decreases with the particle size from 150 μm to 1250 μm. For the smaller particles of 150 μm, it only takes ~10 s to complete the calcination process, while for the larger particles of 1250 μm, the

conversion of the particles is only ~90 wt.% within 80 s. An interesting finding in the work is that when the CO_2 concentration in the gas phase increases from 0 vol.% to 30 vol.%, the decrease in the conversion of limestone particles becomes less obvious with the increase of particle size. This indicates that the effect of CO_2 concentration in the gas phase on the reduction of the calcination rate of small particle limestone is higher than that of large particle size. Furthermore, it can be seen that the results of the prediction model are in good agreement with the experimental values.

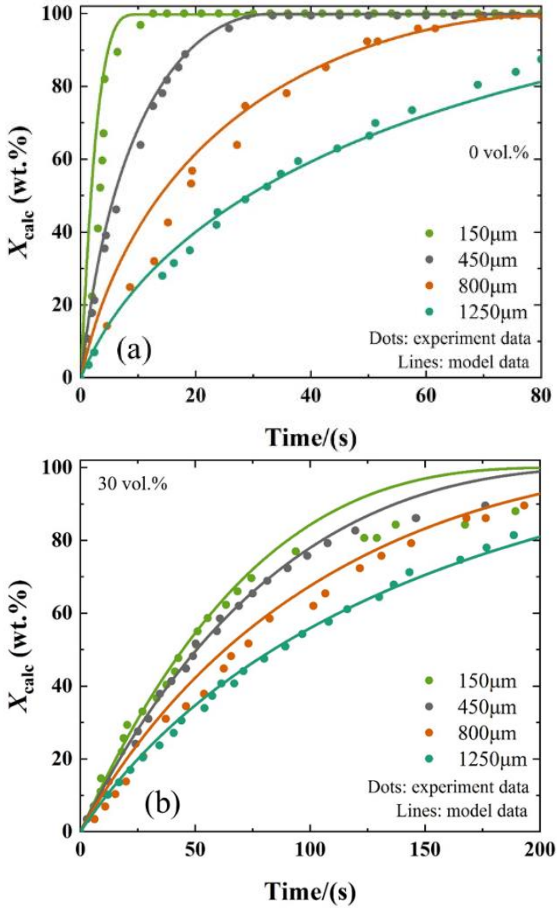

Figure 4. Comparison between the model results and the MFB-TGA experimental data at different particle size under (**a**) 0 vol.%; (**b**) 30 vol.%.

For larger particle sizes, the gas mass transfer resistance is larger both for external and intraparticle diffusion. Thus, the CO_2 partial pressure on the particle surface is higher than for smaller particles. With the continuous progress of the chemical reaction, the change of CO_2 partial pressure on the particle surface under high CO_2 concentration in the gas phase is smaller than that under lower CO_2 concentration, which results in the change of particle conversion with particle size no longer being significant at high CO_2 concentrations.

2.5. Determination of Kinetic Parameters

Based on the comparison of the experimental results with the model established in Section 5, the value of the activation energy can be obtained from the slope of the fitted line, and the value of the pre-exponential factor can be obtained from the vertical intercept of the fitted line in Figure 5. The kinetic parameter calculation is summarized in Table 1. The activation energy of the chemical reaction rate constant k_f is 182 kJ/mol, which indicates that the temperature has an extremely distinct effect on the value of the chemical reaction rate constant in the range of 750–920 °C. Activation energies have been reported to be in the range of 100–230 kJ/mol depending on the specific calcination conditions and the

established model [24]. Escardino et al. [45] obtained an apparent activation energy value of 175 kJ/mol for the direct chemical reaction of thermal calcination. Garcia et al. [19] studied limestone and dolomite, with activation energies ranging from 114–166 kJ/mol. The E values measured in the work are close to those reported by other researchers [19,22,27,29]. The activation energy of the thermodynamic equilibrium constant K_1 in the reaction kinetics in this work is 150 kJ/mol, which is consistent with the value reported by Jose et al. [33]. Other parameters in the model are summarized in Table 1.

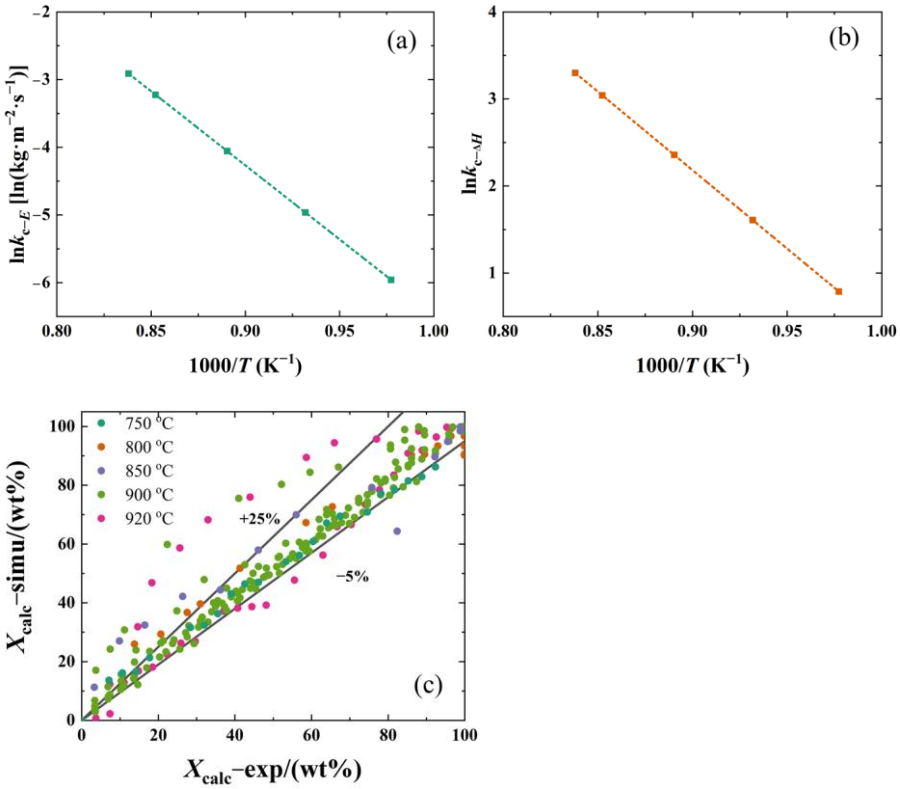

Figure 5. Arrhenius plots to calculate the kinetic parameters: (**a**) $\ln k_{c-E}$ versus 1/T; (**b**) $\ln k_{c-\Delta H}$ versus 1/T; (**c**) comparison of model results to experimental data.

Table 1. Kinetic parameters in the model calculation.

A (kg/m^2/s)	E (kJ/mol)	a (/)	ΔH (kJ/mol)	C_1 (s/K$^{0.75}$)	S_0 (m^2/kg)	ε_0 (/)	$\bar{r}_0$(μm)
5.051×10^6	182	9.99×10^7	150	5×10^{-12}	22.80	0.48	330

Figure 5c compares the model results and the experimental data. Most of the errors between the model and experimental results are between −5% and +20%, indicating that the model can reasonably predict the decomposition conversion within the experimentally investigated range.

3. Discussion

Based on Equation (10), the fraction occupied by *CO_2 in the adsorbed state on the particle surface, θ, is calculated as:

$$\theta = \frac{P_i}{K_2 + P_i} = \frac{P_{eq} - \frac{K_r}{k_c} \cdot (P_{eq} - P_g)}{\frac{P_{eq}}{K_1} + P_{eq} - \frac{K_r}{k_c} \cdot (P_{eq} - P_g)} \quad (1)$$

θ represents the fraction of active sites on the surface of the limestone particles occupied by CO_2 produced by calcination. The relationship between θ and CO_2 partial pressure in

the gas phase is displayed in Figure 6. It can be seen that with the increase in CO_2 partial pressure, the fraction θ occupied by CO_2 on the particle surface gradually increases. That is, the R2 desorption process of the CO_2 produced by calcium carbonate from the particle surface through the reaction R1 is limited by the increase of CO_2 in the gas phase. Especially in the low CO_2 partial pressure stage, θ increases rapidly with the increase of CO_2 partial pressure. When the partial pressure of CO_2 in the gas phase achieves ~30,000 Pa (~30 vol.% at atmospheric pressure) at 900 °C, the fraction θ occupied by active sites on the particle surface increases from 0 to 0.8. However, when the partial pressure of CO_2 in the gas phase is higher than ~60,000 Pa (~60 vol.% at atmospheric pressure), with the increase of the partial pressure of CO_2, θ increases slowly. In this case, the desorption process of CO_2 from the particle surface becomes very slow and the calcination reaction is limited.

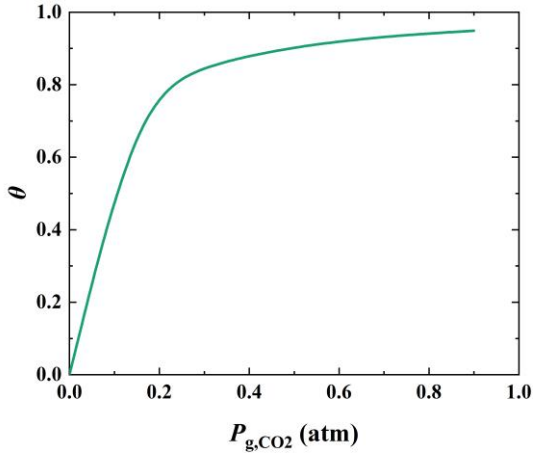

Figure 6. The fraction of surface active sites occupied θ under 900 °C.

Figure 7 shows the change of the occupied fraction θ of active sites on the particle surface under different particle sizes. It can be found that for larger particles, the fraction θ occupied by adsorbed $*CO_2$ on the particle surface increases with the particle size, indicating that the CO_2 desorption rate becomes slower with an increase in particle size. This illustrates that there is a certain correlation between the limestone calcination reaction and particle size, which in turn verifies the limestone calcination model in Section 5. The occupied fraction θ on the particle surface rises rapidly in the initial stage and soon reaches saturation. The variation of particle surface θ with particle size under high CO_2 concentration is smaller than that under low CO_2 concentration, which also leads to the change in particle conversion with particle size no longer being significant.

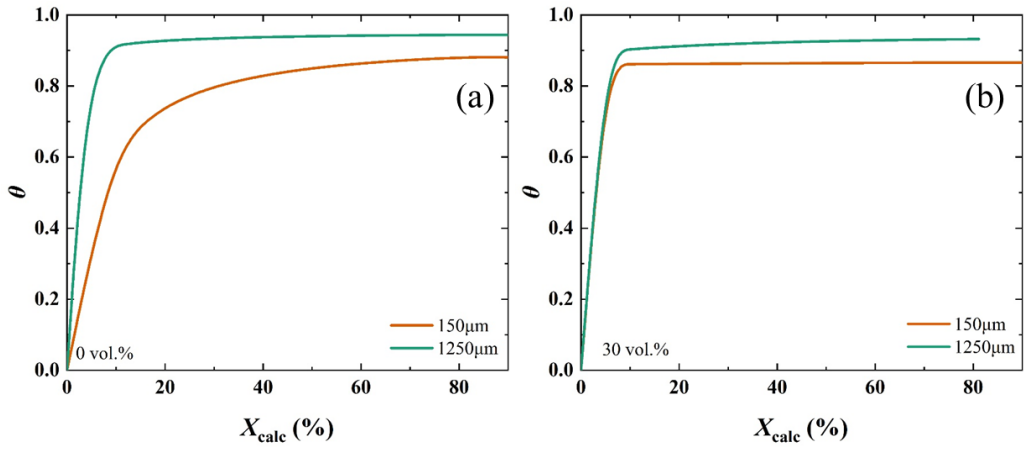

Figure 7. θ on particle surface of different particle sizes under (**a**) 0 vol.% and (**b**) 30 vol.%.

Figure 8a shows the effect of the temperature on the reaction-controlling mechanism calculated using the established model in Section 5. It can be seen that for the limestone calcination process, there is an excellent linear relationship between the consumption rate of particles and the temperature from 600–1050 °C. This reveals that the consumption of limestone particles is mainly controlled by a combination of chemical reactions and gas diffusion in the investigated range.

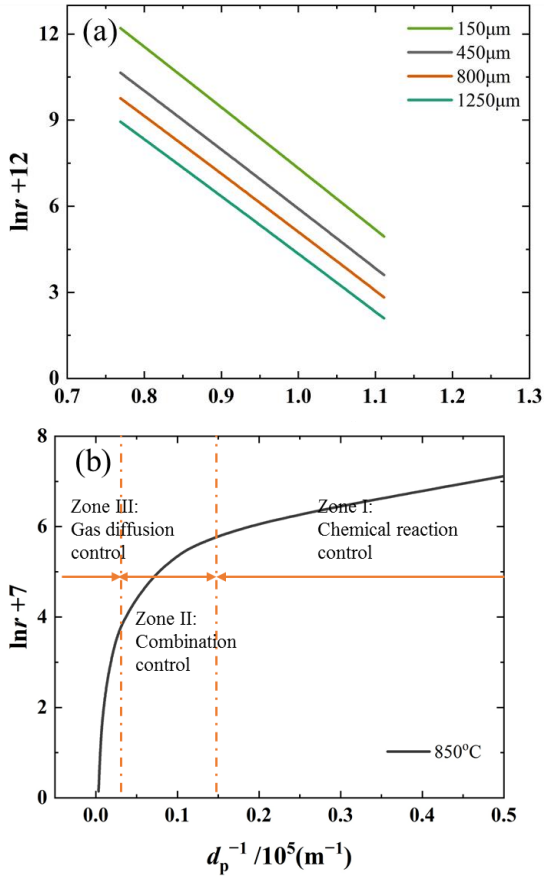

Figure 8. Calculated results of the effect on the limestone calcination reaction controlling mechanism at X_{calc} = 0.5: (**a**) temperature; (**b**) particle size. (*r* is the calcination consumption rate of particles).

Figure 8b shows the effect of the particle size on the limestone calcination reaction controlling mechanism. It can be seen that the consumption rate of limestone and particle size have clear three-zone characteristics. When the particle size is smaller than ~80 μm, the change of the particle size has less effect on the limestone particle consumption rate. In this case, the particle consumption rate is mainly controlled by chemical reactions, referred to as Zone I. While the particle size is larger than ~450 μm, the particle consumption rate varies significantly with particle size; this is referred to as Zone III. At this time, the calcination reaction is mainly controlled by gas diffusion, including the gas external diffusion step and the intraparticle diffusion step. As the particle size increases, the calcination rate decreases rapidly; that is, the gas diffusion resistance within the particle and the external gas diffusion resistance increase rapidly. In the particle size range of 80–450 μm, that is, Zone II, the gas diffusion resistance and chemical reaction resistance are in the same order of magnitude, and the calcination process is controlled by both gas diffusion and chemical reaction.

The above analysis can guide the optimization of limestone particle calcination conditions at different temperatures and CO_2 concentrations in practical applications. The chemical reaction rate, internal diffusion rate and external diffusion rate of the particles are comprehensively considered to determine the appropriate operating temperature and particle size.

4. Experiment

4.1. Microfluidized Bed Thermogravimetric Analysis (MFB-TGA)

A natural limestone from Hubei Province with calcium carbonate content exceeding 99.4% is explored in the work. After crushing and grinding, the limestone is carefully sieved to particle size ranges of 150–200 μm, 450–500 μm, 800–900 μm, and 1250–1410 μm. Each sieving process is repeated three times.

The calcination experiments of limestone are conducted in a microfluidized bed thermogravimetric analysis (MFB-TGA) apparatus, as shown in Figure 9a, which consisted of a quartz reactor, an electric furnace, a gas supply system, and a measurement system [46]. The quartz reactor is designed to be a fluidized bed with an inner diameter of 28 mm, the inner diameter of the top sample inlet of 10 mm, and a porous distribution plate with a thickness of 5 mm to make the air flow evenly into the reactor. The gas supply system consists of mass flow controllers calibrated with a soap bubble flowmeter prior to the experiment, solenoid valves, and gas cylinders. By using a sufficiently thin silicone hose to connect the reactor and the inlet pipe, hard connections can be avoided and interference with the quality signal can be eliminated. The measurement system realizes real-time online monitoring and recording of temperature, pressure and mass signals. The mass signal is the core of the apparatus and is measured with a precise weighing transducer with an accuracy of 1 mg. During the experiment, it is necessary to ensure that no part of the quartz reactor is in contact with the furnace so as not to affect the measurement of the quality signal. The temperature signal is measured with a wireless K-type thermocouple. The pressure difference between the gas inlet and outlet is monitored using a differential pressure sensor to judge the fluidization properties.

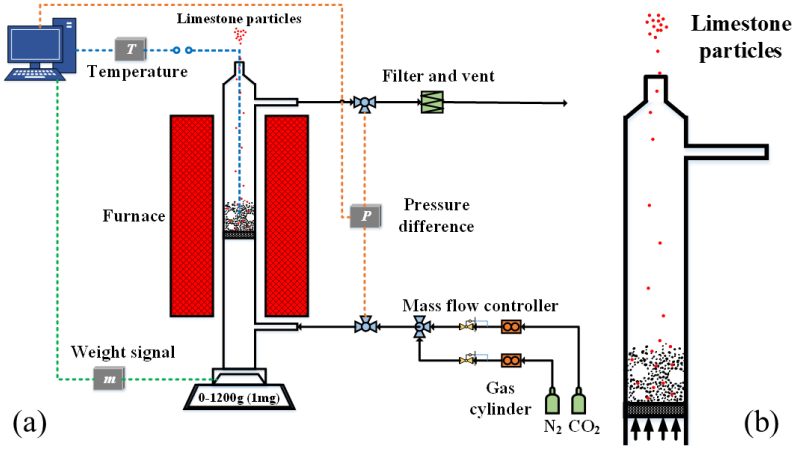

Figure 9. Schematic diagrams of (**a**) the MFB-TGA apparatus and (**b**) the limestone particles being injected into the reactor.

A novel experimental method is proposed and implemented to ensure that limestone particles are calcined under isothermal conditions in the work. As shown in Figure 9b, the limestone particles are injected into the hot sands which are fluidized in the high temperature quartz reactor, and the limestone particles are instantly heated to the reaction temperature and decomposed under the set CO_2 atmosphere. In a typical experiment, ~16 g of quartz sand with a particle size of 300–355 μm is added to the quartz reactor as the inert bed material (black particles in Figure 9b). The reaction gas is passed into the reactor, and the flow rate is ~3 U_{mf} (U_{mf} is the minimum fluidization speed). This indicates that as the temperature increases, the feed gas flow rate should decrease accordingly. The furnace temperature is raised to 850 °C and stabilized for 30 min. The fluctuation of the mass signal within 120 s is ±1 mg in the steady state, as shown in Figure 10a, indicating that the experimental system is highly stable. After that, the limestone particles (red particles in Figure 9b) are quickly injected into the fluidized bed from the top inlet of the reactor, and

the mass increased rapidly by 64 mg within 0.2 s (equal to the mass of injected limestone), as shown in Figure 10b. The limestone particles are blended with the inert bed material in the reactor, heated, and calcined in a fluidizing condition. During the experiment, the mass injected of limestone is 60–70 mg to minimize the effect of mass transfer. Each condition is repeated several times to ensure reproducibility.

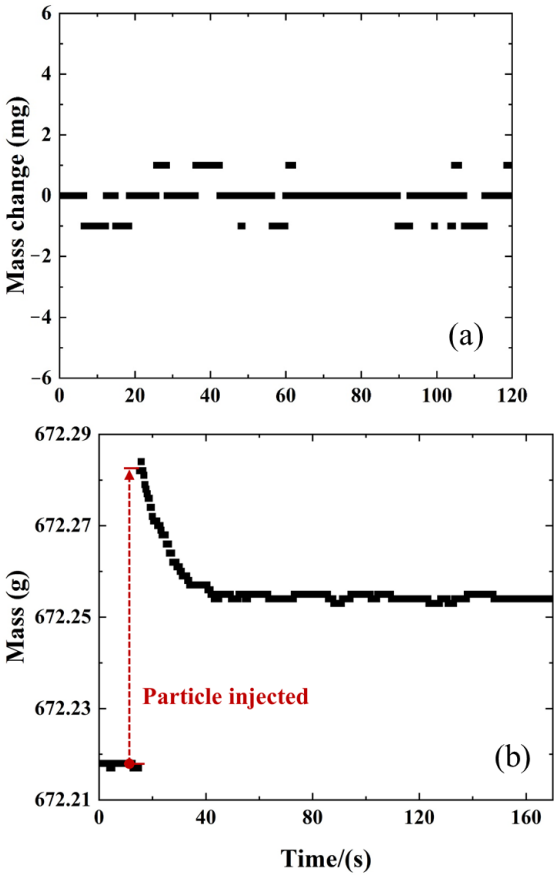

Figure 10. The mass signal of the weighing transducer: (**a**) the initial steady mass before limestone particles are injected; (**b**) real-time mass signal of limestone particles being injected.

4.2. Experimental Condition and Data Evaluation

The calcination characteristics of limestone particles are studied at 750–920 °C in the work. The CO_2 concentration is in the range of 0 and 30 vol.%, and N_2 is the balance gas. The detailed experimental conditions are displayed in Table 2.

Table 2. Experiment condition.

Sample Mass/mg	Particle Size/μm	Temperature/°C	CO_2/%	Superficial Velocity
60–70	150/450/800/1250	750–920	0/30	~3 U_{mf}

The calculation of the conversion of limestone particles depends on the mass value (limestone mass + quartz reactor mass) from the weighing transducer, and the conversion of limestone X_{Calc} is calculated as Equation (2), where $m(t)$ is the real-time mass during the calcination, m_0 is the initial steady mass before limestone particles are added and m_1 is the final steady mass after the decomposition's completion.

$$X_{Calc} = \left(1 - \frac{m(t) - m_0}{m_1 - m_0} \cdot \frac{M_{w,CaO}}{M_{w,CaCO_3}}\right) \cdot \frac{M_{w,CaCO_3}}{M_{w,CO_2}} \times 100\% \quad (2)$$

where $M_{w,CaCO_3}$, $M_{w,CaO}$, and M_{w,CO_2} are the molecular weights of $CaCO_3$, CaO, and CO_2, respectively.

5. Models

The limestone particles are considered to be dense and nonporous spherical particles with an initial radius of r_0, as displayed in Figure 11. Therefore, a shrinking core model is adopted in the work to describe the limestone calcination process. As shown in Figure 11, when the calcination reaction occurs, the calcium carbonate on the surface of the particles is first decomposed, forming a porous calcium oxide shell evenly covering the outer surface. While the reaction occurs, the calcium carbonate core with radius r_2 continues to decompose. It is worth noting that the CO_2 generated from the calcination of the limestone core must pass through the pores of the calcium oxide shell to diffuse to the outer surface, known as intraparticle diffusion. Then, the CO_2 on the outer surface of the particles is transferred into the gas stream through external diffusion. As the reaction continues, the calcium carbonate core inside the particle gradually shrinks, while the outer calcium oxide shell gradually increases until the inner calcium carbonate core is completely consumed and the reaction is completed.

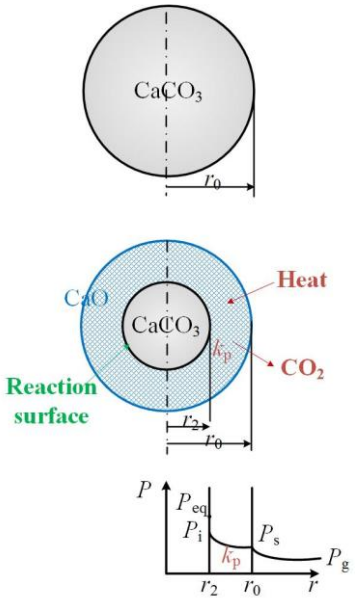

Figure 11. Schematic diagram of the shrinking core model describing the calcination of limestone particles.

According to the geometrical relation shown in Figure 11, the conversion of limestone particles X_{calc} can be calculated as:

$$X_{calc} = \frac{r_0^3 - r_2^3}{r_0^3} \tag{3}$$

Then, the conversion rate of the particles is obtained as:

$$\frac{dX_{calc}}{dt} = -\frac{3r_2^2}{r_0^3}\frac{dr_2}{dt} \tag{4}$$

Based on Equation (3), it is deduced that the correlation of the radius r_2 of the calcium carbonate core and the initial particle radius r_0 is:

$$r_2 = r_0 \cdot (1 - X_{calc})^{1/3} \tag{5}$$

The consumption rate of limestone particle volume is calculated as:

$$\frac{\mathrm{d}V_{\mathrm{CaCO_3}}}{\mathrm{d}t} = 4\pi r_2^2 \frac{\mathrm{d}r_2}{\mathrm{d}t} = -4\pi r_2^2 \cdot \Lambda \cdot V_{\mathrm{CaCO_3}}^{\mathrm{M}} \cdot R_{\mathrm{calc}} \tag{6}$$

where R_{calc} is the chemical reaction rate, $1/\mathrm{s}$; Λ is the active site density at the interface, $\mathrm{mol/m^2}$; and $V_{\mathrm{CaCO_3}}^{\mathrm{M}}$ is the molar volume of calcium carbonate, $\mathrm{m^3/mol}$.

Combining Equations (4)–(6),the conversion of the limestone particle is expressed as:

$$\frac{\mathrm{d}X_{\mathrm{calc}}}{\mathrm{d}t} = \frac{3}{r_0}(1 - X_{\mathrm{calc}})^{2/3} \Lambda \cdot V_{\mathrm{CaCO_3}}^{\mathrm{M}} \cdot R_{\mathrm{calc}} \tag{7}$$

The decomposition process of calcium carbonate is a typical gas–solid surface reaction. In addition to chemical surface reactions, the diffusion of CO_2 through the porous CaO layer and around the particles should be considered in the developed model to reflect the effect of CO_2 concentration. Therefore, in the subsequent derivation, we assume that the surface reaction of spherical calcium carbonate particles occurs through the shrinking core model, and the model of intraparticle and external diffusion processes of CO_2 is established. Finally, combining the above three steps, the expression of the effective rate constant is derived to describe the detailed calcium carbonate decomposition process.

5.1. Calcination Kinetics

Assume an ideal case of the calcination of an infinite calcium carbonate plane under uniform CO_2 partial pressure and temperature conditions. The surface reaction process of calcium carbonate can be described by two steps of chemical calcination and desorption [19,32]. The first step is the chemical calcination of calcium carbonate on the surface, resulting in CO_2 molecules being adsorbed on the surface and occupying active sites. The second step is the desorption of CO_2 molecules from the active site. The two-step calcination process is characterized by reactions R1 and R2 as follows:

$$\underset{1-\theta}{\mathrm{CaCO_3} + *} \overset{\underset{k_{1r}}{k_{1f}}}{\rightleftharpoons} \mathrm{CaO} + \underset{\theta}{* \mathrm{CO_2}} \tag{R1}$$

$$\underset{\theta}{*\mathrm{CO_2}} \overset{\underset{k_{2r}}{k_{2f}}}{\rightleftharpoons} * + \underset{1-\theta \quad P_{\mathrm{i}}}{\mathrm{CO_2}} \tag{R2}$$

where k_{1f}, k_{1r}, k_{2f}, and k_{2r} are the forward and reverse reaction rate constants of R1 and R2, respectively. * is an active site on the particle surface; θ is defined as the fraction of the active site on the particle surface occupied by CO_2. P_{i} is the CO_2 partial pressure at the interface between CaO and $CaCO_3$ inside the particle.

Based on the microscopic reversibility general principle, when the reaction reaches chemical equilibrium, the forward reaction rate of the elementary reaction equal to reverse reaction rate is obtained:

$$\begin{aligned} k_{1f}(1 - \theta_{\mathrm{eq}}) &= k_{1r}\theta_{\mathrm{eq}} \\ k_{2f}\theta_{\mathrm{eq}} &= k_{2r}(1 - \theta_{\mathrm{eq}})P_{\mathrm{eq}} \end{aligned} \tag{8}$$

Then, the CO_2 partial pressure at equilibrium is obtained as:

$$P_{\mathrm{eq}} = \frac{k_{1f}k_{2f}}{k_{1r}k_{2r}} = K_1 K_2 \tag{9}$$

where the subscript eq indicates that the reaction is at equilibrium, and K_1 and K_2 are the thermodynamic equilibrium constants of R1 and R2, respectively.

It is assumed that the adsorbed $*CO_2$ is in a quasi-steady state, and the desorption rate of CO_2 is a generally extremely fast progress compared with the chemical calcination

rate; that is, the control step of calcium carbonate calcination is the reaction R1, and R2 ≈ 0. Therefore, the fraction occupied θ is calculated as:

$$R_2 \approx 0 \Rightarrow \theta \approx \frac{k_{2r}P_{\mathrm{i}}}{k_{2f} + k_{2r}P_{\mathrm{i}}} = \frac{P_{\mathrm{i}}}{K_2 + P_{\mathrm{i}}} \tag{10}$$

The chemical reaction rate of calcium carbonate calcination is also obtained as:

$$R_{\mathrm{calc}} \approx R_1 = k_{1f}\left(1 - \frac{P_{\mathrm{g}}}{P_{\mathrm{eq}}}\right)\frac{1}{1 + K_1 \cdot \frac{P_{\mathrm{i}}}{P_{\mathrm{eq}}}} \tag{11}$$

It can be seen that the above derivation is based on the ideal case of an infinite calcium carbonate plane, while the limestone is actually spherical particles. Therefore, a modification is introduced in Equation (11) in order to choose the one that provided the best fit with the experimental results and given as:

$$R_{\mathrm{calc}} = k_{1f}\left(1 - \frac{P_{\mathrm{g}}}{P_{\mathrm{eq}}}\right)\frac{1}{1 + K_1 \cdot \frac{P_{\mathrm{i}}}{P_{\mathrm{eq}}} \cdot \frac{\bar{r}_0}{r_0}} \tag{12}$$

where $\bar{r}_0$ is the average radius of particles in the investigated range, calculated as 330 μm, and r_0 is the particles' radius.

Combined with Equation (7), the conversion rate of the particles is obtained as:

$$\frac{\mathrm{d}X_{\mathrm{calc}}}{\mathrm{d}t} = \frac{3}{r_0\rho} \cdot k_{\mathrm{c}} \cdot \left(P_{\mathrm{eq}} - P_{\mathrm{g}}\right) \tag{13}$$

$$k_{\mathrm{c}} = k_{1f} \cdot \rho \cdot \Lambda \cdot V^{\mathrm{M}}_{\mathrm{CaCO_3}} \cdot \left(1 - X_{\mathrm{calc}}\right)^{2/3}\frac{1}{P_{\mathrm{eq}} + K_1 P_{\mathrm{i}} \cdot \frac{\bar{r}_0}{r_0}} \tag{14}$$

where k_{c} is the comprehensive chemical reaction rate constant. Combining the constant terms in Equation (14), it is obtained that:

$$k_{\mathrm{c}} = k_f \cdot \left(1 - X_{\mathrm{calc}}\right)^{2/3}\frac{1}{P_{\mathrm{eq}} + K_1 P_{\mathrm{i}} \cdot \frac{\bar{r}_0}{r_0}} \tag{15}$$

where the reaction rate constant k_f is calculated based on the Arrhenius form, and the thermodynamic equilibrium constant K_1 is calculated based on the van't Hoff equation in Equation (15):

$$k_f = k_{1f} \cdot \rho \cdot \Lambda \cdot V^{\mathrm{M}}_{\mathrm{CaCO_3}} = A \cdot e^{-\frac{E}{RT}} \tag{16}$$

$$K_1 = \frac{\Delta S}{R} \cdot e^{-\frac{\Delta H}{RT}} = a \cdot e^{-\frac{\Delta H}{RT}} \tag{17}$$

where A and E are the pre-exponential factor and activation energy, respectively, of k_{f}. ΔS and ΔH are the standard entropy and enthalpy change of the $CaCO_3$ calcination reaction, and a is the pre-exponential factor of K_1. The four kinetic parameters—A, E, a, and ΔH—in the reaction term are parameters to be determined.

The equilibrium concentration of CO_2, P_{eq} is obtained based on the work of Hu et al., Pa [47]:

$$P_{\mathrm{eq}} = 1.826 \times 10^6 \times \exp\left(-19680/T_{\mathrm{p}}\right) \times 10^6 \tag{18}$$

5.2. Intraparticle Diffusion

The diffusion of CO_2 through the calcium oxide layer can be described by Fick's law of diffusion, and the diffusion flow rate of CO_2 is given as:

$$J_{\mathrm{CO_2}} = -4\pi r^2 \cdot D_{\mathrm{e}} \cdot \frac{dC_{\mathrm{CO_2}}}{dr} \tag{19}$$

where C_{CO_2} is the CO_2 concentration in the calcium oxide layer and D_e is the gas diffusion coefficient, which is calculated based on the empirical formula [28]:

$$D_e = 0.00881 T^{1/2} S_0^{-1} \varepsilon_0^2 \tag{20}$$

where S_0 is the initial specific surface area of particles, taken as 22.80 m^2/g, and ε_0 is the initial porosity of the CaO layer, taken as 0.48 according to the work of Wang et al. [43].

The boundary conditions are that:

$$\begin{cases} r = r_2 \; C_{CO_2} = C_i \\ r = r_0 \; C_{CO_2} = C_s \end{cases} \tag{21}$$

Integrate Equation (21) and simplify to obtain:

$$J_{CO_2} = \frac{4\pi D_e (C_i - C_s)}{\frac{1}{r_2} - \frac{1}{r_0}} = 4\pi r_0^2 \frac{D_e (C_i - C_s)}{\frac{r_0}{r_2}(r_0 - r_2)} \tag{22}$$

According to the ideal gas equation of state, combine with Equation (5) to obtain:

$$J_{CO_2} = 4\pi r_0^2 \frac{D_e (P_i - P_s)}{r_0 \frac{[1-(1-X_{calc})^{1/3}]}{(1-X_{calc})^{1/3}} RT} \tag{23}$$

Then the conversion rate of the particles is obtained as:

$$\frac{dX_{calc}}{dt} = \frac{J_{CO_2} \cdot M_{w,CaCO_3}}{m_0} = \frac{3}{r_0 \rho} \cdot k_p \cdot (P_i - P_s) \tag{24}$$

$$k_p = \frac{D_e \cdot M_{w,CaCO_3}}{r_0 \cdot \frac{[1-(1-X_{calc})^{1/3}]}{(1-X_{calc})^{1/3}} RT} \tag{25}$$

where m_0 is the initial mass of the limestone particle and k_p is the gas intraparticle diffusion rate constant.

5.3. External Diffusion

The particle conversion rate due to CO_2 external diffusion from the surface of limestone particle to the main flow is:

$$\frac{dX_{calc}}{dt} = \frac{3}{r_0 \rho} \cdot k_D (P_s - P_g) \tag{26}$$

where k_D is the diffusion coefficient of CO_2 to the bulk atmosphere, which is given based on the work of Field [48] and Graham [49] and related to temperature and particle size:

$$k_{O_2} = C_1 \frac{\left[(T_p + T_g)/2\right]^{0.75}}{d_p} \tag{27}$$

$$k_D = k_{O_2} \sqrt{\frac{M_{w,O_2}}{M_{w,CO_2}}} \tag{28}$$

where T_p and T_g are the particle temperature and gas temperature, respectively; M_{w,O_2} and M_{w,CO_2} are the molecular weights of O_2 and CO_2, respectively; and C_1 is an empirical constant with a value of 5×10^{-12} s·$K^{-0.75}$.

5.4. Calcination Kinetic Model

The effects of chemical reaction, gas intraparticle and external diffusion during limestone calcination are considered in Sections 5.1–5.3. In order to eliminate the unknown

parameters P_i and P_s in Equations (13) and (24), combing Equations (13), (14), (24), (25), and (26) gives:

$$\frac{1}{\frac{3}{r_0\rho}\cdot k_c}\frac{dX_{calc}}{dt}+\frac{1}{\frac{3}{r_0\rho}\cdot k_p}\frac{dX_{calc}}{dt}+\frac{1}{\frac{3}{r_0\rho}\cdot k_D}\frac{dX_{calc}}{dt}=-(P_{eq}-P_i)-(P_i-P_s)-(P_s-P_g)=-(P_{eq}-P_g) \quad (29)$$

Thus, the conversion rate of the limestone particle is:

$$\frac{dX_{calc}}{dt}=\frac{3}{r_0\rho}\cdot K_r\cdot(P_{eq}-P_g) \quad (30)$$

$$K_r=\frac{1}{\frac{1}{k_c}+\frac{1}{k_p}+\frac{1}{k_D}} \quad (31)$$

where K_r is the comprehensive calcination rate constant of the particle. It is worth noting that in Equation (15), the partial pressure of CO_2 at the intraparticle surface of the particle, P_i, is unknown. Thus, P_g is adopted as an approximate substitute in the calculation process.

The flowchart of the calculation algorithm is displayed in Figure 12. The algorithm-solving steps are: (i) initializing the particle parameters, making X_{calc} = 0.0001 to avoid meaningless k_p calculation, and inputting the constant parameters; (ii) calculating the external diffusion rate constant k_D; (iii) calculating the comprehensive chemical reaction rate constant k_c; (iv) calculating the intraparticle diffusion rate constant k_p; (v) updating the particle conversion X_{calc} at time t and then proceeding to the next time step $t + \Delta t$.

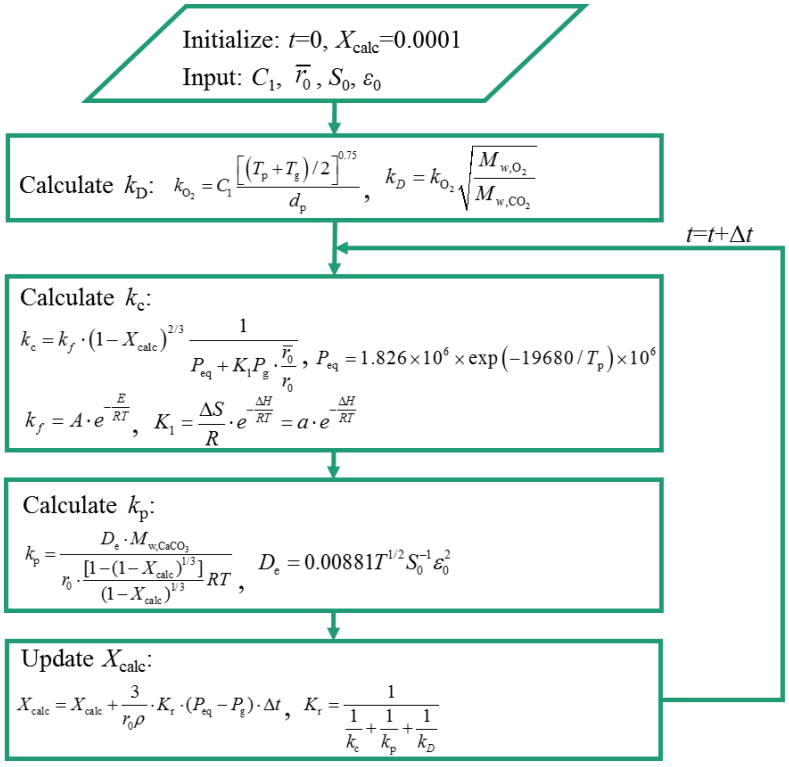

Figure 12. Flowchart of the calculation algorithm.

6. Conclusions

The calcination kinetics of the fluidized limestone particles under rapid heating and isothermal conditions are measured by injecting them into the microfluidized bed thermogravimetric analyzer (MFB-TGA). The calcination characteristics of limestone with different particle sizes are studied in the temperature range of 750–920 °C and the CO_2 concentration of 0 and 30 vol.%. A calcination kinetic model considering surface reaction, CO_2 partial

pressure, particle structure change, and intraparticle and external diffusion is established, and the key parameters of the model are obtained; that is, $A = 5.051 \times 10^6$ kg·m^{-2}·s^{-1}, $E = 182$ kJ/mol, $a = 9.99 \times 10^7$, $\Delta H = 150$ kJ/mol. The results show that it only takes ~10 s to achieve complete conversion at temperatures >900 °C. Increasing the CO_2 concentration in the gas phase severely impairs the calcination rate of the particles. An interesting point is that as the partial pressure of CO_2 increases, the effect of particle size decreases. In the investigated temperature range, the particle consumption is controlled by both the chemical reaction and gas diffusion. The effect of particle size on limestone calcination kinetics presents three-zone characteristics of the reaction controlling mechanism. In Zone I, the particle size is <~80 μm, the particle size has little effect on the consumption rate, and calcination is mainly controlled by chemical reaction. In Zone III, the particle size is >~450 μm, the calcination process is mainly controlled by gas diffusion, and the effect of particle size is significant. In Zone II, in the particle size range of 80–450 μm, the calcination is controlled by both gas diffusion and chemical reaction. The model prediction results are in good agreement with the experimental data, indicating that the experimental results and the calcination model will provide valuable information for the application of CaL technology.

Author Contributions: Conceptualization, D.L. and Z.L.; methodology, D.L., Y.W. and Z.L.; software, D.L.; validation, D.L., Y.W. and Z.L.; formal analysis, D.L. and Z.L.; investigation, D.L.; resources, Z.L.; data curation, D.L. and Z.L.; writing—original draft preparation, D.L.; writing—review and editing, D.L. and Z.L.; visualization, D.L.; supervision, Z.L.; project administration, Z.L.; funding acquisition, Z.L. All authors have read and agreed to the published version of the manuscript.

Funding: This research was supported by National Natural Science Foundation of China (Grant No. 51876095) and supported by the International Joint Mission On Climate Change and Carbon Neutrality.

Data Availability Statement: The data presented in this study are available in the article.

Conflicts of Interest: The authors declare no conflict of interest.

References

1. Han, R.; Wang, Y.; Xing, S.; Pang, C.; Hao, Y.; Song, C.; Liu, Q. Progress in reducing calcination reaction temperature of Calcium-Looping CO_2 capture technology: A critical review. *Chem. Eng. J.* **2022**, *450*, 137952. [CrossRef]
2. Perejón, A.; Romeo, L.M.; Lara, Y.; Lisbona, P.; Martínez, A.; Valverde, J.M. The Calcium-Looping technology for CO_2 capture: On the important roles of energy integration and sorbent behavior. *Appl. Energy* **2016**, *162*, 787–807. [CrossRef]
3. Rivero, M.A.; Rodrigues, D.; Pinheiro, C.I.; Cardoso, J.P.; Mendes, L.F. Solid-gas reactors driven by concentrated solar energy with potential application to calcium looping: A comparative review. *Renew. Sust. Energ. Rev.* **2022**, *158*, 112048. [CrossRef]
4. Qin, C.; He, D.; Zhang, Z.; Tan, L.; Ran, J. The consecutive calcination/sulfation in calcium looping for CO_2 capture: Particle modeling and behaviour investigation. *Chem. Eng. J.* **2018**, *334*, 2238–2249. [CrossRef]
5. Di Giuliano, A.; Gallucci, K. Sorption enhanced steam methane reforming based on nickel and calcium looping: A review. *Chem. Eng. Process.* **2018**, *130*, 240–252. [CrossRef]
6. Blamey, J.; Anthony, E.; Wang, J.; Fennell, P. The calcium looping cycle for large-scale CO_2 capture. *Prog. Energy Combust. Sci.* **2010**, *36*, 260–279. [CrossRef]
7. Hashemi, S.M.; Sedghkerdar, M.H.; Mahinpey, N. Calcium looping carbon capture: Progress and prospects. *Can. J. Chem. Eng.* **2022**, *100*, 2140–2171. [CrossRef]
8. Hornberger, M.; Spörl, R.; Scheffknecht, G. Calcium looping for CO_2 capture in cement plants-pilot scale test. *Energy Procedia* **2017**, *114*, 6171–6174. [CrossRef]
9. Haaf, M.; Stroh, A.; Hilz, J.; Helbig, M.; Ströhle, J.; Epple, B. Process modelling of the calcium looping process and validation against 1 MWth pilot testing. *Energy Procedia* **2017**, *114*, 167–178. [CrossRef]
10. Bui, M.; Adjiman, C.S.; Bardow, A.; Anthony, E.J.; Boston, A.; Brown, S.; Fennell, P.S.; Fuss, S.; Galindo, A.; Hackett, L.A. Carbon capture and storage (CCS): The way forward. *Energy Environ. Sci.* **2018**, *11*, 1062–1176. [CrossRef]
11. Li, Z.; Cai, N.; Huang, Y.; Han, H. Synthesis, experimental studies, and analysis of a new calcium-based carbon dioxide absorbent. *Energy Fuels* **2005**, *19*, 1447–1452. [CrossRef]
12. Rodriguez, N.; Alonso, M.; Grasa, G.; Abanades, J.C. Heat requirements in a calciner of $CaCO_3$ integrated in a CO_2 capture system using CaO. *Chem. Eng. J.* **2008**, *138*, 148–154. [CrossRef]
13. Grasa, G.S.; Abanades, J.C. CO_2 capture capacity of CaO in long series of carbonation/calcination cycles. *Ind. Eng. Chem. Res.* **2006**, *45*, 8846–8851. [CrossRef]

14. Hyatt, E.P.; Cutler, I.B.; Wadsworth, M.E. Calcium carbonate decomposition in carbon dioxide atmosphere. *J. Am. Ceram. Soc.* **1958**, *41*, 70–74. [CrossRef]
15. Khinast, J.; Krammer, G.; Brunner, C.; Staudinger, G. Decomposition of limestone: The influence of CO_2 and particle size on the reaction rate. *Chem. Eng. Sci.* **1996**, *51*, 623–634. [CrossRef]
16. Hills, A. The mechanism of the thermal decomposition of calcium carbonate. *Chem. Eng. Sci.* **1968**, *23*, 297–320. [CrossRef]
17. Borgwardt, R.H. Calcination kinetics and surface-area of dispersed limestone particles. *AlChE J.* **1985**, *31*, 103–111. [CrossRef]
18. Rajeswara, R. Kinetics of calcium carbonate decomposition. *Chem. Eng. Res. Des.* **1989**, *67*, 38–47.
19. Garcıa-Labiano, F.; Abad, A.; De Diego, L.; Gayán, P.; Adánez, J. Calcination of calcium-based sorbents at pressure in a broad range of CO_2 concentrations. *Chem. Eng. Sci.* **2002**, *57*, 2381–2393. [CrossRef]
20. Ylätalo, J.; Parkkinen, J.; Ritvanen, J.; Tynjälä, T.; Hyppänen, T. Modeling of the oxy-combustion calciner in the post-combustion calcium looping process. *Fuel* **2013**, *113*, 770–779. [CrossRef]
21. Szekely, J.; Evans, J. A structural model for gas-solid reactions with a moving boundary. *Chem. Eng. Sci.* **1970**, *25*, 1091–1107. [CrossRef]
22. Ar, I.; Dogu, G. Calcination kinetics of high purity limestones. *Chem. Eng. J.* **2001**, *83*, 131–137. [CrossRef]
23. Escardino, A.; Garcia-Ten, J.; Feliu, C.; Saburit, A.; Cantavella, V. Kinetic study of the thermal decomposition process of calcite particles in air and CO_2 atmosphere. *Ind. Eng. Chem. Res.* **2013**, *19*, 886–897. [CrossRef]
24. Galwey, A.K.; Brown, M.E. Application of the Arrhenius equation to solid state kinetics: Can this be justified? *Thermochim. Acta* **2002**, *386*, 91–98. [CrossRef]
25. Ramezani, M.; Tremain, P.; Doroodchi, E.; Moghtaderi, B. Determination of carbonation/calcination reaction kinetics of a limestone sorbent in low CO_2 partial pressures using TGA experiments. *Energy Procedia* **2017**, *114*, 259–270. [CrossRef]
26. Guler, C.; Dollimore, D.; Heal, G. The investigation of the decomposition kinetics of calcium carbonate alone and in the presence of some clays using the rising temperature technique. *Thermochim. Acta* **1982**, *54*, 187–199. [CrossRef]
27. Dennis, J.; Hayhurst, A. The effect of CO_2 on the kinetics and extent of calcination of limestone and dolomite particles in fluidised beds. *Chem. Eng. Sci.* **1987**, *42*, 2361–2372. [CrossRef]
28. Silcox, G.D.; Kramlich, J.C.; Pershing, D.W. A mathematical model for the flash calcination of dispersed calcium carbonate and calcium hydroxide particles. *Ind. Eng. Chem. Res.* **1989**, *28*, 155–160. [CrossRef]
29. Rao, T.R. Kinetics of calcium carbonate decomposition. *Chem. Eng. Technol.* **1996**, *19*, 373–377. [CrossRef]
30. Fuertes, A.; Marban, G.; Rubiera, F. Kinetics of thermal decomposition of limestone particles in a fluidized bed reactor. *Chem. Eng. Re.s Des.* **1993**, *71*, 421–428.
31. Wang, Y.; Lin, S.; Suzuki, Y. Limestone calcination with CO_2 capture (II): Decomposition in CO_2/steam and CO_2/N_2 atmospheres. *Energy fuels* **2008**, *22*, 2326–2331. [CrossRef]
32. Valverde, J.M.; Sanchez-Jimenez, P.E.; Perez-Maqueda, L.A. Limestone calcination nearby equilibrium: Kinetics, CaO crystal structure, sintering and reactivity. *J. Phys. Chem. C* **2015**, *119*, 1623–1641. [CrossRef]
33. Ramon Fernandez, J.; Turrado, S.; Carlos Abanades, J. Calcination kinetics of cement raw meals under various CO_2 concentrations. *React. Chem. Eng.* **2019**, *4*, 2129–2140. [CrossRef]
34. Barker, R. The reversibility of the reaction $CaCO_3 \rightleftarrows$ CaO+ CO_2. *J. Chem. Technol. Biotechnol.* **1973**, *23*, 733–742. [CrossRef]
35. Calvo, E.G.; Arranz, M.; Leton, P. Effects of impurities in the kinetics of calcite decomposition. *Thermochim. Acta* **1990**, *170*, 7–11. [CrossRef]
36. Valverde, J.M. On the negative activation energy for limestone calcination at high temperatures nearby equilibrium. *Chem. Eng. Sci.* **2015**, *132*, 169–177. [CrossRef]
37. Wang, Y.; Lin, S.; Suzuki, Y. Study of limestone calcination with CO_2 capture: Decomposition behavior in a CO_2 atmosphere. *Energy Fuels* **2007**, *21*, 3317–3321. [CrossRef]
38. Scaltsoyiannes, A.; Lemonidou, A. $CaCO_3$ decomposition for calcium-looping applications: Kinetic modeling in a fixed-bed reactor. *Chem. Eng. Sci. X* **2020**, *8*, 100071. [CrossRef]
39. Lv, G.; Lu, J.; Cai, L.; Xie, X.; Liu, Z. Experimental study on the dynamic process of NO reduction in a precalciner. *Ind. Eng. Chem. Res.* **2011**, *50*, 4366–4372.
40. Khraisha, Y.; Dugwell, D. Coal combustion and limestone calcination in a suspension reactor. *Chem. Eng. Sci.* **1992**, *47*, 993–1006. [CrossRef]
41. Li, Y.; Li, Z.; Wang, H.; Cai, N. CaO carbonation kinetics determined using micro-fluidized bed thermogravimetric analysis. *Fuel* **2020**, *264*, 116823. [CrossRef]
42. Wang, Y.; Li, Z.; Cai, N. Redox reaction kinetics of a Fe-Cu-based oxygen carrier measured with microfluidized bed thermogravimetric analysis. *Energy Fuels* **2022**, *36*, 9672–9686. [CrossRef]
43. Wang, H.; Li, Z.; Li, Y.; Cai, N. Reduced-order model for CaO carbonation kinetics measured using micro-fluidized bed thermogravimetric analysis. *Chem. Eng. Sci.* **2021**, *229*, 116039. [CrossRef]
44. Giammaria, G.; Lefferts, L. Catalytic effect of water on calcium carbonate decomposition. *J. CO_2 Util.* **2019**, *33*, 341–356. [CrossRef]
45. Escardino, A.; Garcia-Ten, J.; Feliu, C. Kinetic study of calcite particle (powder) thermal decomposition: Part I. *J. Eur. Ceram. Soc.* **2008**, *28*, 3011–3020. [CrossRef]
46. Li, Y.; Li, Z.; Liu, L.; Cai, N. Measuring the fast oxidation kinetics of a manganese oxygen carrier using microfluidized bed thermogravimetric analysis. *Chem. Eng. J.* **2020**, *385*, 123970. [CrossRef]

47. Hu, N.; Scaroni, A.W. Calcination of pulverized limestone particles under furnace injection conditions. *Fuel* **1996**, *75*, 177–186. [CrossRef]
48. Field, M.A. Rate of combustion of size-graded fractions of char from a low-rank coal between 1200 K and 2000 K. *Combust. Flame* **1969**, *13*, 237–252. [CrossRef]
49. Graham, T. On the law of the diffusion of gases. *J. Membr. Sci.* **1995**, *100*, 17–21.sss. [CrossRef]